Preprints of the 21st IFAC World Congress (Virtual)
Berlin, Germany, July 12-17, 2020

# A Kriging-based Interacting Particle Kalman Filter for the simultaneous estimation of temperature and emissivity in Infra-Red imaging

**Thibaud Toullier** * **Jean Dumoulin** * **Laurent Mevel** *

* *Univ. Gustave Eiffel, Inria, COSYS-SII, I4S, 35042 Rennes, France*

**Abstract:** Temperature estimation through infrared thermography is facing the lack of knowledge of the observed material's emissivity. The derivation of the physical equations lead to an ill-posed problem. A new Kriged Interacting Particle Kalman Filter is proposed. A state space model relates the measurements to the temperature and the Kalman filter equations yield a filter tracking the temperature over time. Moreover, a particle filter associated to Kriging prediction is interacting with a bank of Kalman filters to estimate the time-varying parameters of the system. The efficiency of the algorithm is tested on a simulated sequence of infrared thermal images.

*Keywords:* Particle filtering, Kalman filtering, Kriging, Thermal Infrared imaging, Physical parameters

## 1. INTRODUCTION

The latest improvements on uncooled infrared detectors for thermal cameras provide new opportunities to derive remotely the temperature of observed objects. In particular, multispectral infrared thermography can be used for the thermal monitoring of civil engineering structures for which data are acquired through a long period in outdoor conditions. However, without any knowledge on the observed object, the temperature can only be exploited relatively. In fact, the derivation of an object's temperature through infrared thermography cannot be done witout the knowledge of the object's intrinsic emissivity radiative property. This temperature and emissivity separation (TES) problem is ill-posed: $N$ spectral measurements require the estimation of $N+1$ variables ($N$ emissivity values and one temperature value). This problem cannot be tackled without adding more knowledge in the equation system Krapez (2011).

By considering only the interaction between the sensor and the observed object, this study aims at exploiting the temporal and spatial characteristics of the measurements to estimate conjointly the emissivity and the temperature. The simultaneous estimation is done by combining an Interacting Particle Kalman Filter (IPKF) Zghal et al. (2014) to track in time the evolution of the temperature as well as estimating the parameters of the model with a Kriging step to decrease the computation time by reducing the number of pixels monitored by the Kalman equations.

Kriged Kalman Filters (KKF) have been previously used in the literature for the estimation of temporal varying spatial fields and sensors placement (Cressie and Wikle (2011); V. Mardia et al. (1998); Baingana et al. (2015); Roy et al. (2018)). In those methods, the parameters of the system are known or estimated through an autoregressive model and the Kriging is performed to interpolate spatial data between measurements points. This paper introduces a new method on which the system parameters are estimated through an IPKF and the Kriging step is not only used for the interpolation of data but also to infer a spatial model onto the system, leading to a Kriging-based Interacting Particle Kalman Filter (KIPKF). Another contribution of this paper is the application of the KIPKF to the TES problem which opens new perspectives toward absolute temperature measurements through infrared thermography.

The radiative transfer equations that reflect the infrared thermography measurement process will be presented first. Then, an Interacting Particle Kalman Filter will be introduced to estimate the missing parameters of the system. A Kriging step will be described to infer a spatial model in the system. Finally, the developed method will be tested on a numerical case and compared to a state of the art method.

## 2. PROBLEM DEFINITION

### *2.1 Infrared thermography*

The radiative heat flux density received at the camera sensor array for a given pixel $(i,j)$ and for a given spectral band $\lambda_i$ under laboratory conditions is given by the following simplified radiative transfer equation:

$$\begin{aligned} L^{(i,j)}_{\text{received}} =& \epsilon^{(i,j)}_{\text{obj}}(\lambda_i) L^{\circ}_{\text{obj}}(T_{\text{obj}}, \lambda_i) \\ &+ (1-\epsilon^{(i,j)}_{\text{obj}}(\lambda_i)) L^{\circ}_{\text{env}}(T_{\text{env}}, \lambda_i) \end{aligned} \tag{1}$$

where $L^{\circ}_{\text{obj}}(T_{\text{obj}}, \lambda_i)$ $(\text{W}\cdot\text{m}^{-2}\cdot\text{sr}^{-1}\cdot\mu\text{m}^{-1})$ represents the self emission governed by Planck's law that depends on temperature and wavelength, Howell et al. (2010):

$$L^{\circ}(T,\lambda) = \frac{C_1}{\lambda^5}\frac{1}{e^{\frac{C_2}{\lambda T}}-1} \tag{2}$$

with $C_1 = 1.191 \times 10^{-16}\,\mathrm{W}\cdot\mathrm{m}^2$ and $C_2 = 1.439 \times 10^{-2}$ $\mathrm{m}\cdot\mathrm{K}$. $\epsilon_{\lambda_i,\mathrm{obj}}$ is the emissivity of the object and $L^{\circ}_{\lambda_i,\mathrm{env}}$ the contribution of the surrounding environment, reflected by the object and neglected in the following. Please note that the emissivity is an intrinsic parameter of a given surface comprised between 0 and 1 which depends on material nature, roughness, angle of observation, wavelength and temperature. In the following and as a first approximation, the surfaces are assumed to follow diffuse emission law and emissivity dependence to temperature can be neglected for the domain of application considered.

### *2.2 Measurement equation*

Let $\mathcal{S} \subset \mathbb{R}^2$ be the image space domain and $\mathscr{T} \subset \mathbb{R}^+$ the time domain. Let also assume that the observed object has a slow varying emissivity value through time. After removing the geometrical coefficients, the irradiance $\gamma(T,\boldsymbol{s},t,\lambda_i)$ received at a given pixel $\boldsymbol{s} \in \mathcal{S}$, a time $t \in \mathscr{T}$ and a spectral band $\lambda_i$ can be written as:

$$\gamma(T,\boldsymbol{s},t,\lambda_i) = \epsilon(\boldsymbol{s},t,\lambda_i)L^{\circ}(T,\lambda_i) \tag{3}$$

With temperature $T$ that implicitely depends on time $t$ and pixel location $\boldsymbol{s}$. This measurement equation can be splitted into two parts: a dynamic component and a stationnary one:

$$\ln(T,\gamma(\boldsymbol{s},t,\lambda_i)) = \underbrace{\ln(\epsilon(\boldsymbol{s},t,\lambda_i))}_{\text{stationnary}} + \underbrace{\ln(L^{\circ}(T,\lambda_i))}_{\text{dynamic}} \tag{4}$$

By using Wien's approximation:

$$\ln(\frac{\gamma(T,\boldsymbol{s},t,\lambda_i)\lambda^5}{C_1}) = \ln(\epsilon(\boldsymbol{s},t,\lambda_i)) - \frac{C_2}{\lambda_i T(\boldsymbol{s},t)} \tag{5}$$

Equation (5) leads to an undetermined system of one equation and two unknowns ($\epsilon$ and $T$). By looking at (5), one can extract two main components of the signal: a time-varying variable $T(\boldsymbol{s},t)$ and an assumed stationnary part $\epsilon(\boldsymbol{s},t,\lambda_i)$. The TES problem can therefore be discretized for a given band $\lambda_i$ as a time-variant system:

$$\begin{cases} x_k(\boldsymbol{s}) &= A_k x_{k-1}(\boldsymbol{s}) \\ y_k(\boldsymbol{s}) &= C x_k(\boldsymbol{s}) + \ln(\epsilon_k(\boldsymbol{s},\lambda_i)) \end{cases} \tag{6}$$

where $x_k(\boldsymbol{s}) = \frac{T_{\mathrm{ref}}}{T_k(\boldsymbol{s})}$, $C = \frac{C_2}{\lambda_i T_{\mathrm{ref}}}$ is known in this application, $T_{\mathrm{ref}}$ is a normalization factor for numeric purposes and $y_k(\boldsymbol{s}) = \ln(\gamma_k(\boldsymbol{s},\lambda_i))$.

The following presented method aims at estimating simultaneously the emissivity and the temperature over an entire image at a given spectral band.

## 3. INTERACTING PARTICLE KALMAN FILTER

### *3.1 Introduction*

The IPKF has been proposed in Zghal et al. (2014) for mechanical system monitoring. The Kalman filter is a key tool for state estimation based on the a priori knowledge of the underlying dynamical model. When the model is not known, it has been shown that a particular filter, where each particle embeds both an instance of the model and the corresponding Kalman filter updated following this specific time-varying model instance. An Interacting Particle Kalman filter is a bank of Kalman filters estimating the states of a linear model, each filter dynamic being driven by a time evolving model, whose dynamics is tracked by a collection of particles.

### *3.2 IPKF algorithm*

The IPKF algorithm, proposed by Zghal et al. (2014) and further improved for noise robustness by Sen et al. (2018b) is a computationally efficient approach to handle state estimation for a time-varying system parameterization. The strategy of decoupling the estimation of states and parameters by using two different filter types for each of them enhances the stability property of the algorithm. This facilitates employing relatively less expensive linear Kalman Filters for linear state estimation while the costly Particle Filter is employed only for parameter estimation. Clearly, IPKF has two parts: i) a PF envelop to estimate the parameters as particles within which ii) a set of nested KFs estimates the states. Both parts are detailed in the following guidelines of Sen et al. (2018a).

***Envelop Particle filter:*** Particle Filtering (PF) deploys a particle approximation by propagating different estimates of the system state matrices $(A, C)$ through a cloud of $N$ independent parameter particles. Different assumptions on the system evolution can be inferred by the time evolution of the different particles. In that paper, only a random walk assumption will be assumed for the parameter evolution. At any arbitrary time step $k$, the evolution of any particle $p$ is basically a random perturbation around its current position:

$$\xi_k^p = \xi_{k-1}^p + r_k^{\xi} \tag{7}$$

where $r_k^{\xi} \sim \mathcal{N}(\delta\xi_k;\sigma_k^{\xi})$ which corresponds to a Gaussian blurring on $\xi_{k-1}^p$ with a shift $\delta\xi_k$ and a spread of $\sigma_k^{\xi}$.

***Nested Kalman filters*** For each particle, the corresponding Kalman state [1] $\boldsymbol{x}_{k-1|k-1}^p$, is updated by the Kalman equations conditioned on the system matrices estimated by particle $p$ in order to predict $\boldsymbol{x}_{k|k-1}^p$. The predicted estimate is subsequently improved using the current measurement $\boldsymbol{y}_k$ to obtain the posterior estimate $\boldsymbol{x}_{k|k}^p$ according to the particle parameter estimate. This process is repeated for all particles yielding a set of posterior estimate for states $\{\boldsymbol{x}_{k|k}^p; \quad \text{for all } p = 1, 2, \cdots, N_p\}$ with $N_p$ the number of particles. Finally, each particle weight is updated using the likelihood of the innovation. The weights are subsequently used to update the prior statistics of the particles by the Bayes rule.

### *3.3 IPKF equations for the TES problem*

Based on (6), the IPKF equations can be derived. The objective is to track the temperature evolution $(x_k(\boldsymbol{s}))$ through time. However, the parameters $A_k$ and $\ln(\epsilon(\boldsymbol{s},\lambda_i))$

[1] $\boldsymbol{x}_{i|j}$ represents estimate of the random variable $\boldsymbol{x}$ at the $i^{th}$ time instant provided the measurement including and upto time instant $j$.

are unknowns and therefore estimated through the PF. The particle $\boldsymbol{\xi}_k^p$ can be defined as:

$$\boldsymbol{\xi}_k^p(\boldsymbol{s}) = \left(a_k^p, \boldsymbol{\alpha}_k^p(\boldsymbol{s})^T\right)^T \tag{8}$$

where $a_k^p \in \mathbb{R}$ is a scalar that describes the temperature evolution through time and the spectral emissivity is represented by $\boldsymbol{\alpha}_k^p$ a vector of length $N_b$ the number of bands considered:

$$\boldsymbol{\alpha}_k^p(\boldsymbol{s}) = \left(\alpha_{i,k}^p(\boldsymbol{s})\right)_{1\leq i\leq N_b} = \left(\ln\left(\epsilon_k^p\left(\boldsymbol{s},\lambda_i\right)\right)\right)_{1\leq i\leq N_b} \tag{9}$$

(6) and (9) yield the state-space model of a given particle, considering dynamic and observation noises:

$$\begin{cases} x_{k+1}^p(\boldsymbol{s}) & = a_k^p x_k^p(\boldsymbol{s}) + v_k \\ \boldsymbol{y}_k^p(\boldsymbol{s}) & = \boldsymbol{\alpha}_k^p(\boldsymbol{s}) + \boldsymbol{C} x_k^p(\boldsymbol{s}) + \boldsymbol{w}_k \end{cases} \tag{10}$$

where $v_k$ and $\boldsymbol{w}_k$ are independent Gaussian white noises with covariance matrices denoted by $\Sigma_v$ and $\boldsymbol{\Sigma}_w$.

***Prediction and correction*** Based on (10), let note $\hat{x}_{k|k}^p$ the estimate of the system's state at time $k$ and $\hat{x}_{k|k-1}^p$ the predicted estimate at time $k$ before correction for a given particle $p$. For estimating the system's state over time, given the measurements $(\boldsymbol{y}_i)_{0\leq i<k}$, the estimate $\hat{x}_{k|k-1}^p$ and covariance matrix $\hat{\Sigma}_{k|k-1}^p$ can be written:

$$\begin{cases} \hat{x}_{k|k-1}^p(\boldsymbol{s}) & = a_k^p \hat{x}_{k-1|k-1}^p(\boldsymbol{s}) \\ \Sigma_{k|k-1}^p(\boldsymbol{s}) & = \left(a_k^p\right)^2 \Sigma_{k-1|k-1}^p(\boldsymbol{s}) + \Sigma_v \end{cases} \tag{11}$$

Similarly, the correction step can be derived with the Kalman equations:

$$\begin{cases} \boldsymbol{i}_k^p(\boldsymbol{s}) & = \boldsymbol{y}_k(\boldsymbol{s}) - \boldsymbol{C}\hat{x}_{k|k-1}^p(\boldsymbol{s}) - \boldsymbol{\alpha}_k^p(\boldsymbol{s}) \\ \boldsymbol{S}_k^p(\boldsymbol{s}) & = \boldsymbol{C}\Sigma_{k|k-1}^p(\boldsymbol{s})\boldsymbol{C}^T + \boldsymbol{\Sigma}_w \\ \boldsymbol{K}_k^p(\boldsymbol{s}) & = \Sigma_{k|k-1}^p(\boldsymbol{s})\boldsymbol{C}^T\left(\boldsymbol{S}_k^p(\boldsymbol{s})\right)^{-1} \\ \hat{x}_{k|k}^p(\boldsymbol{s}) & = \hat{x}_{k|k-1}^p(\boldsymbol{s}) + \boldsymbol{K}_k^p(\boldsymbol{s})\boldsymbol{i}_k^p(\boldsymbol{s}) \\ \Sigma_{k|k}^p(\boldsymbol{s}) & = \Sigma_{k|k-1}^p(\boldsymbol{s}) - \boldsymbol{K}_k^p(\boldsymbol{s})\boldsymbol{C}\Sigma_{k|k-1}^p(\boldsymbol{s}) \end{cases} \tag{12}$$

***Particles update*** The particle approximation $\hat{\boldsymbol{\xi}}_k(\boldsymbol{s}) = \sum_{p=1}^{N_p} w_{k-1}^p \boldsymbol{\xi}_k^p(\boldsymbol{s})$ can be derived from Zghal et al. (2014). The likelihood criterion $p(\boldsymbol{y}_k(\boldsymbol{s})|\boldsymbol{\xi}_k^p(\boldsymbol{s}))$ is given by:

$$p(\boldsymbol{y}_k(\boldsymbol{s})|\boldsymbol{\xi}_k^p(\boldsymbol{s})) = \mathcal{N}\left(\boldsymbol{\alpha}_k^p(\boldsymbol{s}) + \boldsymbol{C}\hat{x}_{k|k-1}^p(\boldsymbol{s}), \boldsymbol{S}_k^p(\boldsymbol{s})\right) \tag{13}$$

The weights of the particles is therefore updated as a classical PF algorithm using:

$$w_k^p = \frac{w_{k-1}^p p(\boldsymbol{y}_k(\boldsymbol{s})|\boldsymbol{\xi}_k^p(\boldsymbol{s}))}{\sum_{p=1}^{N_p} w_{k-1}^p p(\boldsymbol{y}_k(\boldsymbol{s})|\boldsymbol{\xi}_k^p(\boldsymbol{s}))} \tag{14}$$

Then, resampling is done as in Sen et al. (2018a). This algorithm is performed on each pixel $\boldsymbol{s}$.

## 4. KRIGED INTERACTING PARTICLE-KALMAN FILTER (KIPKF)

The previous introduced IPKF enables the tracking of the temperature through time as well as the estimation of the involved parameters. However, such algorithm requires an important amount of particles on each pixel to get satisfying results. Therefore, the processing time of many images measurements is considerable. As a consequence, the IPKF is rewritten in space and a Kriging step is added to achieve three goals:

- Improve the convergence of the algorithm by using a spatial covariance model
- Reduce the computation time by using the Kriging spatial interpolation
- Can be run on a set of single band images

Some previous KKF have been introduced and described previously in the literature where parameters are either assumed to be known or estimated through an autoregressive model as in V. Mardia et al. (1998); Roy et al. (2018). In this study, the IPKF estimates the parameters of the model on the fly. The IPKF is applied only on a subset of the pixels, then the Kriging step is used to infer a spatial model into the system and thus reduce the effective number of explicitely estimated parameters. This approach is slightly different from the traditional approaches, where the Kriging is used to interpolate sparse data, whereas here the total number of estimated parameters for an image is deduced from the subset of the computed estimates.

### *4.1 Kriging*

Kriging is a spatial interpolation method that provides estimates at unknown locations based on sampled ones, Matheron et al. (1962). Let $\mathscr{S} \subset \mathcal{S}$ be the measurement domain ($\text{Card}(\mathscr{S}) = N_L$) and $\mathscr{S}^* \subset \mathcal{S}$ be the spatial domain where the points on which the estimation is to be made are located such as $\mathscr{S} \cup \mathscr{S}^* = \mathcal{S}$.

***Variogram*** Let $\boldsymbol{s} \in \mathscr{S}$ a spatial point with its associated measurement $y(\boldsymbol{s})$. Consider now the measurement at point $\boldsymbol{s}+\boldsymbol{h}$, $\boldsymbol{h} \in \mathbb{R}^2$. The variogram is defined as the expectation of the random variable $(y(\boldsymbol{s}) - y(\boldsymbol{s}+\boldsymbol{h}))^2$ Howarth (1979). Since in practice only one realization of the couple $(y(\boldsymbol{s}), y(\boldsymbol{s}+\boldsymbol{h}))$ is known, the hypothesis behind the modelization of the variogram is to assume that the variogram only depends on the modulus and direction $h$ and not its location $\boldsymbol{s}$. Therefore, the empirical variogram is defined as:

$$2\gamma(\boldsymbol{h}) = \frac{1}{N(\boldsymbol{h})}\sum_{i=1}^{N(\boldsymbol{h})}\left(y(\boldsymbol{s_i}) - y(\boldsymbol{s_i}+\boldsymbol{h})\right)^2 \tag{15}$$

where $N(\boldsymbol{h})$ represents the number of points separated by a vector $\boldsymbol{h}$ in $\mathscr{S}$. Based on the measurements points, an experimental variogram can be computed on which a covariance theoretical model is fitted.

***Universal Kriging (UK)*** Let assume that the spatial field to be interpolated ($\epsilon$) is the sum of a trend function $\mu : \boldsymbol{s} \in \mathcal{S} \rightarrow \mu(\boldsymbol{s}) \in \mathbb{R}$ and a centered square-integrable process $Z$ of known covariance (from variogram):

$$\epsilon(\boldsymbol{s}) = \mu(\boldsymbol{s}) + Z(\boldsymbol{s}) \tag{16}$$

Let $\boldsymbol{s}^* \in \mathscr{S}^*$ and $\boldsymbol{S} = (\boldsymbol{s}_i)_{1\leq i\leq N_L}$. One can assume that the trend $\mu(\boldsymbol{s})$ is unknown and of the form $\mu(\boldsymbol{s}) = \sum_{i=1}^q \beta_i f_i(\boldsymbol{s})$ where $(f_i)_{1\leq i\leq q}$ is a given basis function. The objective of the UK is therefore to get the prediction on $\mathscr{S}^*$ as well as estimating the coefficients $\beta_i$ on the fly, see Roustant and Deville (2014).

### *4.2 Space-time model formulation*

In this section, a space-time model is derived from (5) and (6) and formulated in space instead of wavelength. First, the stationnary and dynamic part of the system are separated as $\boldsymbol{v_{s,k}}$ and $\boldsymbol{v_{d,k}}$ respectively. The measurement equation is

$$\tilde{\boldsymbol{y}}_{\boldsymbol{k}}(\lambda_i) = \boldsymbol{v_{s,k}}(\lambda_i) + C(\lambda_i)\boldsymbol{v_{d,k}} + \boldsymbol{\nu_k} \tag{17}$$

where the process noise $\boldsymbol{\nu_k} \sim \mathcal{N}(0, \boldsymbol{\Sigma_{\nu,k}})$ and with $C(\lambda_i) = \frac{C_2}{\lambda_i T_{\text{ref}}}$, $\boldsymbol{v_{s,k}}(\lambda_i) = \ln(\epsilon_k(\boldsymbol{S}, \lambda_i))$, $\boldsymbol{v_{d,k}} = \frac{T_{\text{ref}}}{\boldsymbol{T_k}(\boldsymbol{S})}$ and $\tilde{\boldsymbol{y}}_{\boldsymbol{k}}(\lambda_i) = \ln(\boldsymbol{\gamma_k}(\boldsymbol{S}, \lambda_i))$. Let the spatially stationary field $\boldsymbol{v_{s,k}}$ follow a random process with $\boldsymbol{\mu_\epsilon}$ its spatial expectation and $\boldsymbol{\Sigma_\epsilon}$ its spatial covariance matrix for a given spectral band. In order to retrieve the previously presented Kalman Filter equations, $\boldsymbol{v_{s,k}}$ is firtsly interpreted as a noise term in the equation, see Roy et al. (2018):

$$\begin{aligned}\tilde{\boldsymbol{y}}_{\boldsymbol{k}}(\lambda_i) - \boldsymbol{\mu_\epsilon}(\lambda_i) =& C(\lambda_i)\boldsymbol{v_{d,k}} \\ &+ (\boldsymbol{v_{s,k}}(\lambda_i) - \boldsymbol{\mu_\epsilon}(\lambda_i)) + \boldsymbol{\nu_k}\end{aligned} \tag{18}$$

The measurement model equation is derived from (18):

$$\hat{\boldsymbol{y}}_{\boldsymbol{k}}(\lambda_i) = C(\lambda_i)\boldsymbol{v_{d,k}} + \boldsymbol{e_{s,k}}(\lambda_i) \tag{19}$$

$$\text{with} \begin{cases} \hat{\boldsymbol{y}}_{\boldsymbol{k}}(\lambda_i) & = \tilde{\boldsymbol{y}}_{\boldsymbol{k}}(\lambda_i) - \boldsymbol{\mu_\epsilon}(\lambda_i) \\ \boldsymbol{e_{s,k}}(\lambda_i) & = (\boldsymbol{v_{s,k}}(\lambda_i) - \boldsymbol{\mu_\epsilon}(\lambda_i)) + \boldsymbol{\nu_k} \\ \boldsymbol{\Sigma_e} & = \boldsymbol{\Sigma_\epsilon}(\lambda_i) + \boldsymbol{\Sigma_{\nu,k}} \end{cases}$$

Similarly to (10), with the process noise $\boldsymbol{\eta_k} \sim \mathcal{N}(0, \boldsymbol{\Sigma_\eta})$, the resulting state-space model is:

$$\begin{cases} \boldsymbol{v_{d,k}} & = \boldsymbol{A_k}\boldsymbol{v_{d,k}} + \boldsymbol{\eta_k} \\ \hat{\boldsymbol{y}}_{\boldsymbol{k}}(\lambda_i) & = C(\lambda_i)\boldsymbol{v_{d,k}} + \boldsymbol{e_{s,k}}(\lambda_i) \end{cases} \tag{20}$$

where $\boldsymbol{A_k} = a_k \boldsymbol{I}$ and $\boldsymbol{\Sigma_\eta}$ are diagonal matrices for simplification (the evolution of the temperature is the same at all points). This state-space model is updated each time new incoming data are gathered through the IPKF. To ensure the convergence of the Kalman filter, the algorithm is started at the beginning of the day (when $0 < a_t < 1$). The algorithm is applied for single spectral band images.

### *4.3 Priors and particle update*

By looking at (19), it can be seen that priors on $\boldsymbol{\mu_\epsilon}$ and $\boldsymbol{\Sigma_\epsilon}$ are needed. $\boldsymbol{\Sigma_\epsilon}$ can be approximated from the initial data at time $k = k_0$, an initial guess $\boldsymbol{T_k} = \boldsymbol{T_{k_0}}$ assuming that thermal equilibrium is reached, by using a variogram model. The assumption that the spatial emissivity covariance is almost constant through time is done (an object with a relatively high emissivity compared to the others on the scene will preserve this relative difference through time). Then, $\boldsymbol{\mu_\epsilon}$ is estimated by using the IPKF algorithm with a first prior also obtained with $\boldsymbol{T_k} = \boldsymbol{T_{k_0}}$. The particle $\boldsymbol{\xi}_k^p$ becomes:

$$\boldsymbol{\xi}_k^p(\lambda_i) = \left(a_k^p, \boldsymbol{\mu_\epsilon}(\lambda_i)^T\right)^T \tag{21}$$

An additional hypothesis is performed. The weights of the particles are updated by assuming that locally (in a given neighborhood) the temperature is homogeneous. Estimated measurements at the locations $(\boldsymbol{s}_i)_{1 \leq i \leq N_L}$ and their neighborhoods are derived by using the kriged emissivity on the neighborhood of $\boldsymbol{s}_i$ and assuming that the temperature in this neighborhood is the same as the temperature in $\boldsymbol{s}_i$. The likelihood of the particle is then derived by comparing those estimations to incoming measurements.

### *4.4 Final algorithm*

To summarize, an IPKF is tracking the dynamic component $\boldsymbol{v_{d,k}}$, whose model $\boldsymbol{\xi}_k^p(\lambda_i) = \left(a_k^p, \boldsymbol{\mu_\epsilon}(\lambda_i)^T\right)^T$ is estimated by the PF. $\boldsymbol{\mu_\epsilon}$ is the mean of stochastic spatial field $\boldsymbol{v_{s,k}}$ on the subset spatial domain $\mathscr{S}$. The covariance model of this spatial domain can be deduced from the fit of a variogram model at the beginning of the algorithm with a given initial prior on $T$, assumed to be constant as in this paper or recomputed over time. The Kriging equations are then used to reconstruct $\boldsymbol{v_{s,k}}$ for the whole image $\mathcal{S}$. The temperature is then deduced at every pixel.

## 5. NUMERICAL APPLICATION

To test the algorithm, a numerical simulation of the observed radiosities through an IR camera has been performed by using a thermal radiative exchanges simulation software Toullier et al. (2019). A target made of four different materials properties has been built. The emissivity profiles (see Fig. 1) are taken from real measurements and the temperature evolution of the target is taken from thermocouples measurements at ground during two days of January 2017. The temperature profile is decimated from the thermocouples measurements to get a sampling rate of 12 min. Four different spectral bands are used: [1.5; 3]µm, [3; 5]µm, [8; 10]µm and [10; 12]µm.

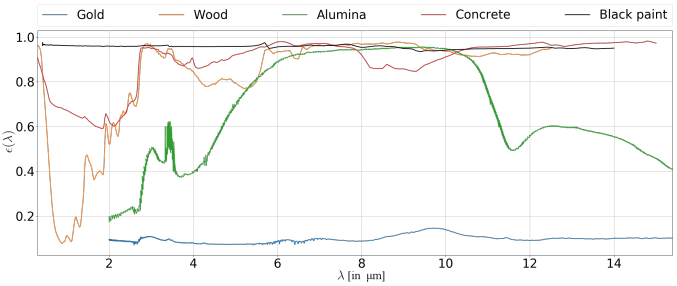


Fig. 1. Emissivity spectrum of the target materials

An example of a simulated image measurement is given in Fig. 2 at one time step.

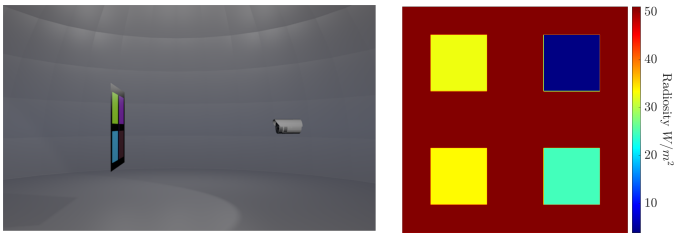


Fig. 2. Left: visible image of the simulation scene. Right: result example of a simulated infrared image for a frame at 293.15 K and the others materials at 278.35 K

## 6. COMPARISON WITH STATE OF THE ART

### *6.1 Description of the bench*

For TES problem, a comparison of the KIPKF method with two other methods is proposed with a sequence of *in-situ* infrared thermography simulated image observations.

***MCMC*** A metaheuristic applied to the TES problem from Ash and Meola (2016) has been implemented. MCMC is run on a single pixel at a single time $k$. The prior on the emissivity is taken as a normal law centered in 0.5 with 0.5 standard deviation. The prior on the temperature is a normal law centered in 273.15 K and 5 K standard deviation.

***IPKF*** For evaluating the Kriging contribution, the previously presented IPKF has been used. However, to improve the performances, an additional criterion has been added. This criterion uses the first derivative in wavelength of the measurement:

$$\frac{\partial \boldsymbol{y_k}(\lambda)}{\partial \lambda} = \frac{1}{\boldsymbol{\epsilon}(\lambda)} \frac{\mathrm{d}\boldsymbol{\epsilon}(\lambda)}{\mathrm{d}\lambda} + \frac{C_2}{\boldsymbol{T_k}(\boldsymbol{s})\lambda^2} \tag{22}$$

### *6.2 Numerical results*

***MCMC*** Results are shown for the alumina material after 10000 iterations and approximately 20 min of computation time for one single pixel at one single instant $t$. One can see on Fig. 3 that the estimated emissivity value matches the average of the initial emissivity value on the spectral band. Fig. 4 shows the estimated temperature at the end of the algorithm where a shift from 273.15 K to the true temperature can be observed. If the algorithm converges to the ground truth values, the required processing time is considerable for only one pixel at one sample result.

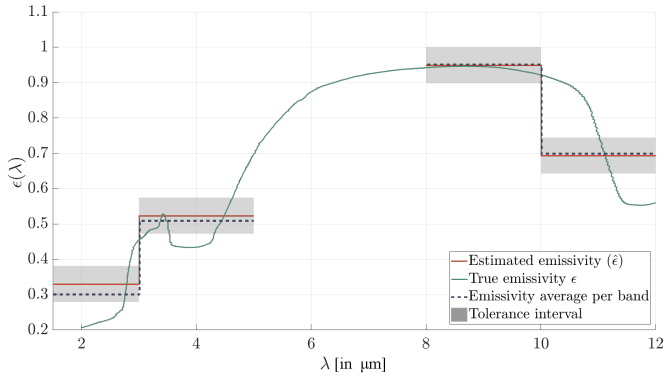


Fig. 3. MCMC: estimated emissivity in orange, original profile in green and in dashed blue the average of the original profile on the different bands of interest.

***IPKF*** Due to the additional hypothesis on the first derivative of the emissivity, simultaneous estimation leads to poor results for multispectral data. However, supplementary retrievals have been done on simulated hyperspectral data. Fig. 5 shows this simultaneous estimation for one pixel and 200 samples after 5 min of computation. In fact, the shape of the emissivity is retrieved leading to a good tracking of the temperature over time. However, the emissivity retrieval stall at the both sides which is due to

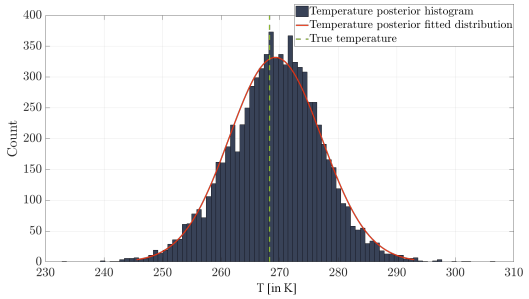


Fig. 4. Temperature posterior after 10000 iterations. The distribution mean in red shifted from 273.15 K toward the true temperature in green.

the fact that the discrete derivative assumption does not work for the first and last points of the profile. This method is therefore promising for hyperspectral applications.

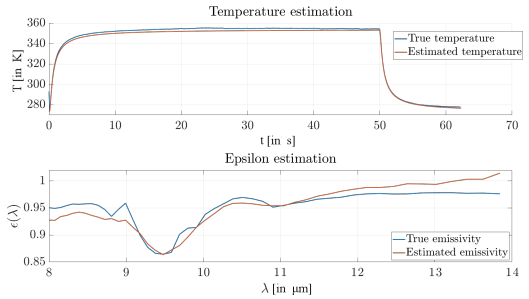


Fig. 5. IPKF on hyperspectral data. The emissivity profile shape is retrieved and the temperature tracked through time, close to the ground truth value.

### *6.3 KIPKF numerical results*

Fig. 6 shows the result of the Kriging step at initialization. Note that the points in $\mathscr{S}$ have been taken only in the material region, due to the fact that in the simulation the temperature of the frame is kept constant, only the materials have a dynamic temperature.

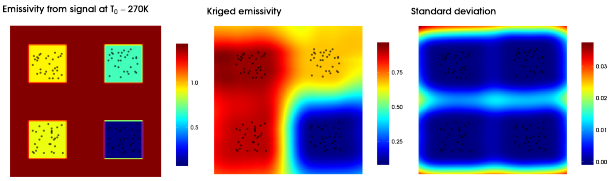


Fig. 6. KIPKF: Kriging model with $T = T_0 = 270$ K. From left to right: the emissivity map from the measurements at $t_0$ and $T_0 = 270$ K, the kriged emissivity and the resulting standard deviation. The black dots correspond to the $N_L$ measurement points in $\mathscr{S}$

The algorithm is then applied on the whole temporal samples of the spectral band [10; 12]µm: 200 images of 545×545 pixels. The computation time was approximately 15 min and results are presented in Fig. 7 and Fig. 8. The different materials can be distinguished from the emissivity map. Moreover, the absolute difference between the estimated emissivity and the ground truth one does not exceed 0.06. The estimated temperature is finally homogeneous on the different materials leading to a difference of less than 3 K

in average. Fig. 8 shows the temperature Kalman estimate over time for a given pixel.

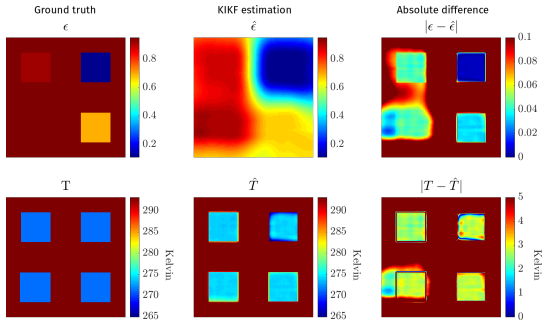


Fig. 7. Example of the simultaneous estimation at a given time. The first row represents the emissivity and second one the temperature. For each row, from left to right: the ground truth, the estimation and the absolute difference between truth and estimate.

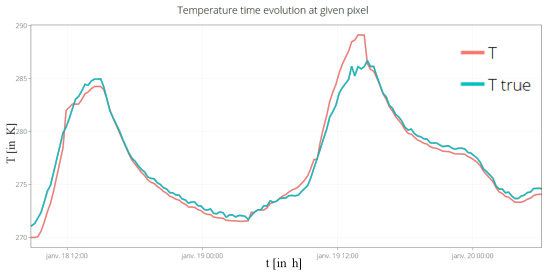


Fig. 8. KIPKF: Result of the temperature estimation through time for a given pixel.

### *6.4 Computational time burden*

Though improvements could be done on each algorithm implementation, the following times give a relative scale between all algorithms. The values are reduced to one given pixel at one instant and one wavelength. The MCMC took $\approx 5$ min, IPKF $\approx 0.002$ s and KIPKF $\approx 0.000\,06$ s.

## 7. CONCLUSION

In this paper, a new method called Kriged Interacting Particle Kalman Filter is proposed and applied to the temperature-emissivity separation problem. The physical thermal radiatives equations have been firstly described by a time-varying system. Then, the IPKF equations have been derived. If the IPKF complies with an hyperspectral system, the narrowed-band hypothesis is inconsistent with multispectral data. As a consequence, a Kriging step has been added to the IPKF to benefit from the spatial characteristics of the signal. The simultaneous estimation of the temperature and emissivity of the observed object on simulated data yields promising results toward absolute temperature estimation by multispectral infrared thermography. This numerical application shows that even if the KIPKF is a consequent method, the computation time is reduced. By its genericity, this filter could be extended to others applications, but further work on robustness is neeeded for application on real data.

## ACKNOWLEDGEMENTS

The support of French Region Bretagne is acknowledged.

## REFERENCES

Ash, J.N. and Meola, J. (2016). Temperature-emissivity separation for LWIR sensing using MCMC. In *Algorithms and Technologies for Multispectral, Hyperspectral, and Ultraspectral Imagery XXII*, volume 9840, 98401O. International Society for Optics and Photonics. doi:10.1117/12.2223263.

Baingana, B., Dall'Anese, E., Mateos, G., and Giannakis, G.B. (2015). Robust kriged Kalman filtering. In *2015 49th Asilomar Conference on Signals, Systems and Computers*, 1525–1529. doi:10.1109/ACSSC.2015.7421400.

Cressie, N.A.C. and Wikle, C.K. (2011). *Statistics for Spatio-Temporal Data*. Wiley Series in Probability and Statistics. Wiley, Hoboken, N.J.

Howarth, R.J. (1979). (A. G.) Journel and (Ch. J.) Huijbregts. Mining Geostatistics. *Mineralogical Magazine*, 43(328), 563–564. doi:10.1180/minmag.1979.043.328.34.

Howell, J., Siegel, R., and Pinar, M. (2010). *Thermal Radiation Heat Transfer*. CRC Press, 5th edition.

Krapez, J.C. (2011). Radiative Measurements of Temperature. In *Thermal Measurements and Inverse Techniques*, Heat Transfer. CRC Press, Boca Raton, FL. OCLC: ocn587104377.

Matheron, G., Blondel, F., and Bureau de recherches géologiques et minières (France) (1962). *Traité de géostatistique appliquée. Tome I Tome I*. Technip, Paris. OCLC: 491866302.

Roustant, O. and Deville, Y. (2014). (Re)Dice Packages for Computer Experiments. In *Troisièmes rencontres R*. Montpellier, France.

Roy, V., Simonetto, A., and Leus, G. (2018). Spatio-Temporal Field Estimation Using Kriged Kalman Filter (KKF) with Sparsity-Enforcing Sensor Placement. *Sensors*, 18(6), 1778. doi:10.3390/s18061778.

Sen, S., Crinière, A., Mevel, L., Cérou, F., and Dumoulin, J. (2018a). Correntropy based IPKF filter for parameter estimation in presence of non-stationary noise process. *IFAC-PapersOnLine*, 51(24), 420–427. doi:10.1016/j.ifacol.2018.09.611.

Sen, S., Crinière, A., Mevel, L., Cérou, F., and Dumoulin, J. (2018b). Seismic-induced damage detection through parallel force and parameter estimation using an improved interacting Particle-Kalman filter. *Mechanical Systems and Signal Processing*, 110, 231. doi:10.1016/j.ymssp.2018.03.016.

Toullier, T., Dumoulin, J., and Mevel, L. (2019). Étude et développement d'un simulateur d'échanges radiatifs dans des scènes 3D statiques et dynamiques surveillées par thermographie infrarouge. In *SFT 2019 - 27eme congrès français de thermique*, 1–8. Nantes, France.

V. Mardia, K., Goodall, C., J. Redfern, E., and Alonso, F. (1998). The Kriged Kalman Filter. *TEST: An Official Journal of the Spanish Society of Statistics and Operations Research*, 7, 217–282. doi:10.1007/BF02565111.

Zghal, M., Mevel, L., and Del Moral, P. (2014). Modal parameter estimation using interacting Kalman filter. *Mechanical Systems and Signal Processing*, 47(1-2), 139–150. doi:10.1016/j.ymssp.2012.11.005.